2006

A Two-Dimensional Simulation Model for Reciprocating Compressors with Automatic Valves

Fred F. S. Matos
Embraco

Carlos J. Deschamps
Federal University of Santa Catarina

Alvaro Toubes T. Prata
Federal University of Santa Catarina

A TWO-DIMENSIONAL SIMULATION MODEL FOR RECIPROCATING COMPRESSORS WITH AUTOMATIC VALVES

F.F.S. MATOS[1], C.J. DESCHAMPS[2], A.T. PRATA[2]

[1]EMBRACO S.A., Product and Process Technology Management,
Joinville, SC, Brazil
Francisco_F_Matos@embraco.com.br

[2]Federal University of Santa Catarina, Department of Mechanical Engineering,
Florianopolis, SC, Brazil
deschamps@polo.ufsc.br

ABSTRACT

A two-dimensional differential methodology is developed to simulate the whole operating cycle of a small refrigeration reciprocating compressor, accounting for the in-cylinder flow. Such compressors adopt automatic valves in which the flow dictates the pressure distribution on the reed surface and, consequently, affects its dynamics. Here, the time dependent flow field through the discharge valve and its dynamics are coupled and solved simultaneously. A one-degree of freedom model is adopted for the valve motion and a finite volume methodology is employed to solve the compressible turbulent flow that prevails in the cylinder and through the valve. Results for the flow field, reed dynamics and indicator diagram are presented to demonstrate the capability of the model.

1. INTRODUCTION

Figure 1 presents a schematic view of a reciprocating compressor and the indicator diagram for a typical cycle. When the piston moves downwards, it reaches a position where low-pressure vapor is drawn in through the suction valve, which is opened automatically by the pressure difference between the cylinder and the suction chamber. The vapor keeps flowing in during the suction stroke as the piston moves towards the bottom dead center (BDC), filling the cylinder volume with vapor at suction pressure, p_s. After reaching the BDC, the piston starts to move in the opposite direction, the suction valve is closed, the vapor is trapped, and its pressure rises as the cylinder volume decreases. Eventually, the pressure reaches the pressure in the discharge chamber, p_d, and the discharge valve is forced to open. After the opening of the discharge valve, the piston keeps moving towards the top dead center (TDC), represented by point A. The suction and discharge processes do not take place at constant pressure due to the dynamics of the valves and the restriction imposed by the valve passage areas. This appears on the indicator diagram, with compression continuing after pressure p_d is reached and the same happening for the expansion stroke after pressure p_s is reached.

Several compressor simulation methodologies are available in the literature. For instance, Soedel (1972) presented a model to thermodynamically evaluate the performance of compressors under cyclical conditions, using integral relations for conservation of mass and energy, and a dynamic model for valves. Morel *et al.* (1988) developed a compressor simulation model to predict component temperatures and flow in suction and discharge systems. Pérez-Segarra *et al*. (1994) proposed a finite volume numerical procedure to simulate the transient compressible one-dimensional flow in the compressor, according to an implicit formulation.

Automatic valves of hermetic compressors open and close depending on the pressure difference between the cylinder and the suction/discharge chamber, established by the piston motion. Once the valves are open, the pressure flow field affects the resultant force acting on the reed. Therefore, in order to obtain an optimum valve system, it is crucial to understand the effects of the phenomena associated with the flow on the valve dynamics. Several studies available in the literature related to automatic valves either model the valve dynamics in detail but pay little attention to the description of the flow field (Khalifa and Liu, 1998), or focus on the fluid mechanics without considering the coupling between valve motion and pressure distribution on the reed (Deschamps *et al*., 1996).

More recently, Matos *et al.* (2002) presented a numerical methodology to explore the interaction between valve dynamics and fluid flow. By prescribing a periodic velocity profile at the entrance of the valve orifice, and solving the governing equations via the finite volume technique, the flow field was obtained. From the pressure on the reed the resultant force was determined and a one-degree of freedom dynamic model was employed to solve the reed acceleration, velocity and displacement.

The main objective of this study is to offer a two-dimensional model to simulate the complete compression cycle of a reciprocating compressor, including the turbulent flow inside the cylinder and through the discharge valve.

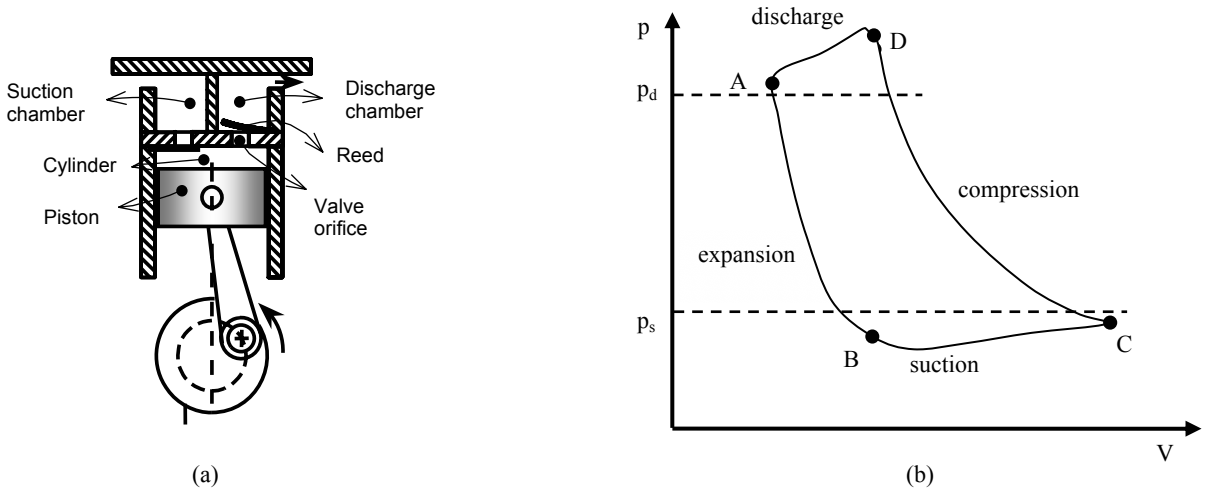

Figure 1: Schematic diagram of a reciprocating compressor and its indicator diagram.

2. MATHEMATICAL MODEL

2.1 Fluid flow

The flow is solved through the Reynolds-averaged Navier-Stokes equations (RANS), in which the value of a computed variable represents an ensemble average over many engine cycles at a specified spatial location. By writing turbulent stresses through the concept of eddy viscosity, the conservation equations for mass, momentum and energy can be written as follows:

a) Mass conservation

$$\frac{\partial \rho}{\partial t}+\frac{\partial \rho u}{\partial x}+\frac{1}{r}\frac{\partial \rho r v}{\partial r}=0 \tag{1}$$

b) Momentum conservation in the axial (x) direction

$$\begin{aligned}\frac{\partial \rho u}{\partial t}+\frac{\partial \rho u u}{\partial x}+\frac{1}{r}\frac{\partial \rho r v u}{\partial r}=&-\frac{\partial p}{\partial x}+\frac{\partial}{\partial x}\left(\mu_{eff}\frac{\partial u}{\partial x}\right)+\frac{1}{r}\frac{\partial}{\partial r}\left(\mu_{eff}\, r\frac{\partial u}{\partial r}\right)+\frac{\partial}{\partial x}\left(\mu_t\frac{\partial u}{\partial x}\right)+\frac{1}{r}\frac{\partial}{\partial r}\left(\mu_t\, r\frac{\partial v}{\partial x}\right)+\\&+\frac{1}{3}\frac{\partial}{\partial x}\left(\mu_{eff}\vec{\nabla}.\vec{V}\right)-\frac{\partial}{\partial x}\left(\mu_t\vec{\nabla}.\vec{V}\right)\end{aligned} \tag{2}$$

c) Momentum conservation in the radial (r) direction

$$\begin{aligned}\frac{\partial \rho v}{\partial t}+\frac{\partial \rho u v}{\partial x}+\frac{1}{r}\frac{\partial \rho r v v}{\partial r}=&-\frac{\partial p}{\partial r}+\frac{\partial}{\partial x}\left(\mu_{eff}\frac{\partial v}{\partial x}\right)+\frac{1}{r}\frac{\partial}{\partial r}\left(\mu_{eff}\, r\frac{\partial v}{\partial r}\right)+\frac{\partial}{\partial x}\left(\mu_t\frac{\partial u}{\partial r}\right)+\frac{1}{r}\frac{\partial}{\partial r}\left(\mu_t\, r\frac{\partial v}{\partial r}\right)-\frac{\mu_{eff}v}{r^2}\\&+\frac{1}{3}\frac{\partial}{\partial r}\left(\mu_{eff}\vec{\nabla}.\vec{V}\right)-\frac{\partial}{\partial r}\left(\mu_t\vec{\nabla}.\vec{V}\right)\end{aligned} \tag{3}$$

d) Energy conservation

$$\frac{\partial \rho T}{\partial t}+\frac{\partial \rho u T}{\partial x}+\frac{1}{r}\frac{\partial r \rho v T}{\partial r}=-p\vec{\nabla}.\vec{V}+\frac{\partial}{\partial x}\left[\left(\frac{\gamma}{c_v}+\frac{c_p}{Pr_t}\frac{\mu_t}{c_v}\right)\frac{\partial T}{\partial x}\right]+\frac{1}{r}\frac{\partial}{\partial r}\left[r\left(\frac{\gamma}{c_v}+\frac{c_p}{Pr_t}\frac{\mu_t}{c_v}\right)\frac{\partial T}{\partial r}\right] \tag{4}$$

In the previous equations, γ is the fluid thermal conductivity and Pr_t is the turbulent Prandtl number, considered here to be 0.9. The effective viscosity μ_{eff} (= $\mu + \mu_t$) is comprised of the molecular viscosity, μ, and the eddy viscosity, μ_t, being evaluated with the RNG k-ε model:

$$\mu_{eff}=\mu\left[1+\sqrt{\frac{C_\mu}{\mu}}\frac{k}{\sqrt{\varepsilon}}\right]^2 \tag{5}$$

The turbulent kinetic energy, k, and its dissipation rate, ε, are obtained through their transport equations:

$$\frac{\partial \rho k}{\partial t}+\frac{\partial \rho u k}{\partial x}+\frac{1}{r}\frac{\partial r \rho v k}{\partial r}=\frac{\partial}{\partial x}\left[\left(\mu+\alpha\mu_t\right)\frac{\partial k}{\partial x}\right]+\frac{1}{r}\frac{\partial}{\partial r}\left[r\left(\mu+\alpha\mu_t\right)\frac{\partial k}{\partial r}\right]+\mu_t S^2-\rho\varepsilon-\rho\varepsilon 2M_t^2 \tag{6}$$

$$\frac{\partial \rho \varepsilon}{\partial t}+\frac{\partial \rho u \varepsilon}{\partial x}+\frac{1}{r}\frac{\partial r \rho v \varepsilon}{\partial r}=\frac{\partial}{\partial x}\left[\left(\mu+\alpha\mu_t\right)\frac{\partial \varepsilon}{\partial x}\right]+\frac{1}{r}\frac{\partial}{\partial r}\left[r\left(\mu+\alpha\mu_t\right)\frac{\partial \varepsilon}{\partial r}\right]+C_{\varepsilon 1}\frac{\varepsilon}{k}\mu_t S^2-C_{\varepsilon 2}\frac{\rho\varepsilon^2}{k}-\rho R+C_{\varepsilon 3}\rho\varepsilon\vec{\nabla}.\vec{V} \tag{7}$$

where C_μ , $C_{\varepsilon 1}$, $C_{\varepsilon 2}$, $C_{\varepsilon 3}$ are equal to 0.0845, 1.42, 1.68 and – 0.373, respectively. On the other hand, M_t (=$k^{1/2}$/c) is defined as the turbulence Mach number, with c being the speed of sound. The terms $\rho\varepsilon 2M_t^2$ and $C_{\varepsilon 3}\rho\varepsilon\vec{\nabla}.\vec{V}$ in equations (6) and (7) are added to correct turbulence levels in the presence of flow compressibility. A detailed discussion on both terms can be found in El Tahry (1983) and Sarkar and Balakrishnan (1990). Finally, the parameters α and R are obtained from the following expressions:

$$\left|\frac{\alpha-1.3929}{\alpha_o-1.3929}\right|^{0.6321}\left|\frac{\alpha+2.3929}{\alpha_o+2.3929}\right|^{0.3679}=\frac{\mu}{\mu_{eff}}\quad;\qquad R=\frac{C_\mu\xi^3\left(1-\xi/\xi_0\right)}{1+\beta\xi^3}\frac{\varepsilon^2}{k} \tag{8}$$

where $\alpha_o = 1.0$, $\beta = 0.012$, $\xi = Sk/\varepsilon$, $\xi_o \approx 4.38$ and $S^2 = 2S_{ij}S_{ij}$, with S_{ij} being the rate of strain tensor. For simplicity, the perfect gas hypothesis was adopted in the state equation required to complete the equation system. An important hypothesis used in this study is that density fluctuations are negligible when compared to velocity fluctuations. Hence, the effect of density variation on the flow is only accounted for through its spatial and temporal variations.

2.2 Valve Dynamics

The dynamics of reeds can be expressed in a simplified way, using a one-degree of freedom model as follows:

$$m\ddot{\delta}_1+C\dot{\delta}_1+K\delta_1=F-F_0 \tag{9}$$

where F_0 is a pre-load force acting on the reed and F is the force resulting from the flow pressure distribution on the reed surface. The valve stiffness and damping coefficients, K and C, respectively, as well as the valve mass, m, are determined experimentally.

As illustrated in Fig. 2, in this study the reed is considered to be parallel to the valve seat. In order to solve Eq. (9) for the valve lift δ_1, force F has to be evaluated from the pressure field created by the flow through the valve as follows:

$$F=\int_0^{D/2} p\,2\pi\,r\,dr \tag{10}$$

It should be mentioned that for the discharge valve, the valve lift was limited to 0.9 mm and a booster was set to act when the valve displacement was 0.3 mm. Because the flow through the suction valve is not numerically solved, force F has to be obtained via the effective force area, A_{ef}.

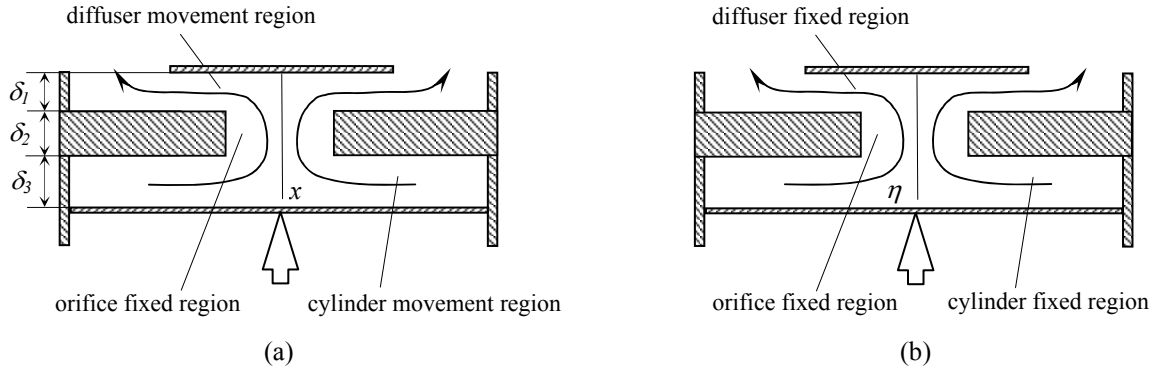

Figure 2: Coordinate system transformation: a) physical domain; b) computational domain.

3. NUMERICAL METHODOLOGY

3.1 Moving coordinate system

Since both the piston and the valves are in motion, it was considered appropriate to solve the governing equations with a moving coordinate system, in which the physical domain is transformed into a computational domain that remains unchanged regardless of any surface motion. Both physical and computational domains are illustrated in Fig. 2. In the moving coordinate system the axial coordinate, x, of the inertial system is replaced by a new axial coordinate, η, as follows:

$$\eta = \frac{x(t)}{\delta_1(t)}; \qquad \eta = x; \qquad \eta = \frac{x(t) - \left[\delta_1(t) + \delta_2\right]}{\delta_3(t)} \tag{11}$$

where subscripts 1, 2 and 3 represent the domain length, in the x direction, of the diffuser, passage orifice and cylinder, respectively. Because the physical domain has two moving regions and a fixed region, in the case of the orifice, for computational reasons, it was preferable to keep the reed fixed and let the seat move. However, this makes no difference whatsoever regarding the physical model.

By using a generic variable ϕ, the differential transport equations for the moving coordinate system can be expressed through a single form:

$$\frac{1}{\delta}\frac{\partial \rho\delta\phi}{\partial t} + \frac{1}{\delta}\frac{\partial \rho\tilde{u}\phi}{\partial \eta} + \frac{1}{r}\frac{\partial \rho r v\phi}{\partial r} = \frac{1}{\delta}\frac{\partial}{\partial \eta}\left(\frac{\Gamma^{\phi}}{\delta}\frac{\partial \phi}{\partial \eta}\right) + \frac{1}{r}\frac{\partial}{\partial r}\left(r\Gamma^{\phi}\frac{\partial \phi}{\partial r}\right) + \overline{S^{\phi}} \tag{12}$$

Therefore, ϕ is equal to 1 when representing mass conservation, u and v for linear momentum conservation, and T for energy conservation. On the other hand, S^{ϕ} and Γ^{ϕ} are the respective source terms and diffusion coefficients for each quantity. For instance, for Eq. (1), S^{ϕ} and Γ^{ϕ} are equal to zero.

When solving the flow in the diffuser domain, in Eq. (12) δ corresponds to the instantaneous valve lift δ_1, which is a result of the valve dynamics. For the feeding orifice no transformation is necessary and, therefore, δ = 1. However, in the cylinder domain δ is equal to the gap between piston and cylinder head, δ_3.

The moving coordinate η varies from 0 to 1 in the diffuser region, from δ_1 to $(\delta_1+\delta_2)$ in the feeding orifice and from 0 to 1 in the region between the piston and cylinder head. In equation (12) the axial velocity component, u, was replaced by the axial velocity $\tilde{u}$ $(= u - u_g)$, which is the flow velocity in relation to the moving coordinate η, where u_g is the instantaneous velocity of the coordinate η, given by one of the following

$$u_g = \left(\frac{\partial x}{\partial t}\right)_{\eta,r} = \eta\frac{\partial \delta_1}{\partial t} = \eta\dot{\delta}_1; \qquad u_g = 0; \qquad u_g = \left(\frac{\partial x}{\partial t}\right)_{\eta,r} = \eta\frac{\partial \delta_3}{\partial t} = \eta\dot{\delta}_3 \tag{13}$$

according to the solution domain being considered. In Eq. (13) $\dot{\delta}_1$ and $\dot{\delta}_3$ are the instantaneous velocity of the reed and piston, respectively.

3.2 Boundary Conditions

At the solid walls all velocity components were taken to be zero, except at the surfaces of the reed and piston where u represents their corresponding velocity values; i.e. $\dot{\delta}_1$ and $\dot{\delta}_3$, respectively. Concerning boundary conditions for the energy equation, a value of 90 ^oC was prescribed for the wall temperature. For the turbulence quantities k and ε, rather than prescribing a condition at the walls, they were calculated in the control volume adjacent to the wall following a two-layer based non-equilibrium wall-function.

At the valve outlet, a boundary condition for pressure was prescribed. In this respect, if the flow is entering the domain, the temperature at the boundary is considered to be that in the discharge chamber; otherwise a parabolic flow condition is employed. Finally, at the valve axis (r = 0) the normal velocity component and the normal gradients of all other quantities were set to zero.

3.3 Solution Procedure

A finite volume methodology was employed to integrate the partial differential equations governing the flow, with a fully implicit approximation for transient terms. Staggered control volumes were adopted for velocity components. Unknown quantities at the control volume faces were estimated using the QUICK interpolation scheme. A segregate approach was employed to solve the equations and the coupling between pressure and velocity was handled through the SIMPLEC algorithm.

The solution domain was discretized with a computational grid with 110x90 (x, r) volumes. Grid refinement was specifically adopted in regions where high gradients are expected to occur in the flow field. Further details on this issue and on the computational domain dimensions can be found in Matos *et al.* (2002).

The differential equation for the valve dynamics, Eq. (9), was solved by considering the force F to be constant during each time step. As seen above, in the case of the discharge valve, F is obtained from the flow pressure distribution on the reed surface. However, for the suction valve the force F and the mass flow rate were obtained with reference to effective force area A_{ef} and effective flow area A_{ee}, respectively.

The iterative procedure evaluates flow properties for each time step until convergence is reached, which is ascertained by examining whether the compressor operation conditions are cyclically repeated. A time step corresponding to 0.01 rad was employed when the valves were closed and 0.002 rad otherwise. Using these time steps, 4 cycles were required to establish a periodic condition, the process taking approximately 78 hours on a computer with a single Pentium IV 3 GHz processor.

4. RESULTS

The present methodology was applied to simulate a small hermetic refrigeration compressor. Figure 3 shows how pressure at the cylinder wall varies according to the crankshaft angle, during the discharge process. In order to clarify the main phenomena affecting the pressure level inside the cylinder during the opening of the discharge valve, results for vector velocity and pressure level contours are presented in Fig. 4 for five crankshaft positions ωt $(= 2\pi f)$: ωt = 2.56 (a); 2.67 (b); 2.78 (c); 2.99 (d) and 3.13 (e) rad. Figure 4a indicates the precise location of the pressure monitoring at the cylinder wall used to construct the indicator diagram of Fig. 3.

With reference to Figs. 3 and 4, each of the aforementioned points can be associated with the following events during the compressor stroke: (a) valve has just opened; (b) valve continues to open and the cylinder pressure is near its highest value; (c) valve is still opening and the pressure has dropped; (d) valve is closing and pressure has increased; (e) valve is returning to the valve seat and pressure is decreasing.

On examining the results, the performance of the valve system can also be analyzed. For instance, it is possible to precisely identify when the valve opens. According to Fig. 3, after the valve is open the pressure keeps rising up to point (b) due to the flow restriction brought about by a small valve lift and a recirculating flow region on the valve seat.

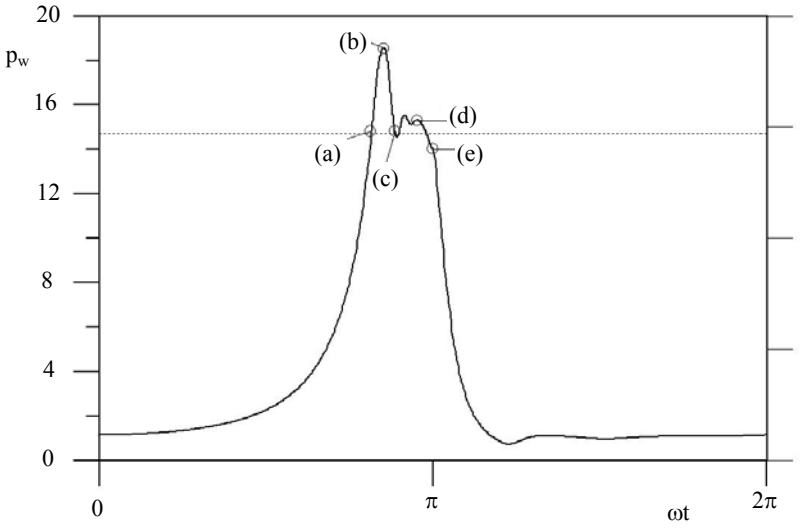

Figure 3: Result for the indicator diagram.

The pressure increase to a level above that of the discharge chamber, indicated by point (a), is linked to distinct aspects: i) stiction force between reed and valve seat; ii) valve inertia; iii) increase in stiffness and natural frequency due to the presence of a booster; iv) flow restriction imposed by the valve. The first two effects are present when the valve is closed. In this simulation, the opening of the valve occurred when the cylinder pressure reached 15 bar.

The discharge valve continues to open and, when the lift is great enough, the cylinder pressure starts to drop down to point (c). Although the flow recirculating region is still present on the valve seat, as can be seen in Fig. 4c, it is a small fraction of the flow passage area. From this crankshaft position the pressure is seen to increase again, point (d). This occurs for two reasons: i) increase in viscous dissipation of flow, due to the narrow clearance between the piston and the cylinder head; ii) closing motion of the valve, restricting the flow passage area.

It is interesting to note that, when the valve is almost closed, the piston has not yet reached the top center crankshaft position. In this case, the viscous dissipation effect in the cylinder clearance can be observed from the results for the isobars. As can be seen in Fig. 4d, there is a pressure drop of approximately 0.5 bar between the cylinder wall and the valve orifice.

For the compressor model here considered, the top dead center (TDC) is reached at a crankshaft angle of 3.10 rad. Since point (e) represents an angle of 3.13 rad, in this position the piston has already started the expansion stroke, originating an abrupt pressure drop in the cylinder that acts to close the discharge valve. Depending on the valve dynamics, some back flow can occur before the valve is totally closed, lowering the volumetric efficiency of the compressor. This important aspect is captured by the simulation under study.

Finally, Fig. 5 shows results for the indicator diagram given by the integral formulation developed by Ussyk (1984) and by the differential model presented here. As can be seen, the overpressures during the discharge process predicted by the two models are quite different. For instance, the integral methodology is not able to predict the second pressure rise in the cylinder. This can be attributed to a better description of the discharge process given by

the differential formulation, with respect to both the reed dynamics and the flow through the valve. In fact, the present methodology offers the potential to explore other fundamental aspects of the compression process, such as heat transfer inside the cylinder.

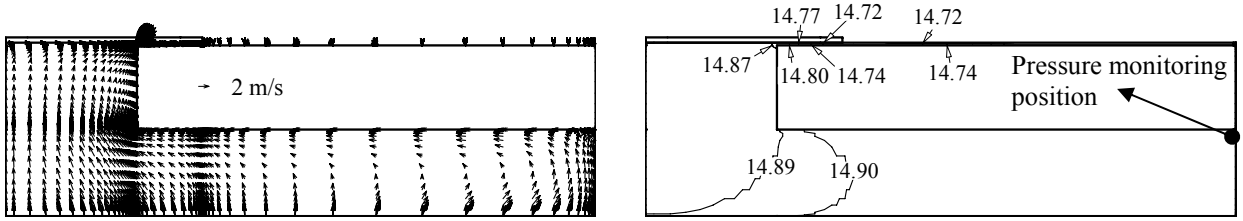

(a) $\omega t = 2.56$.

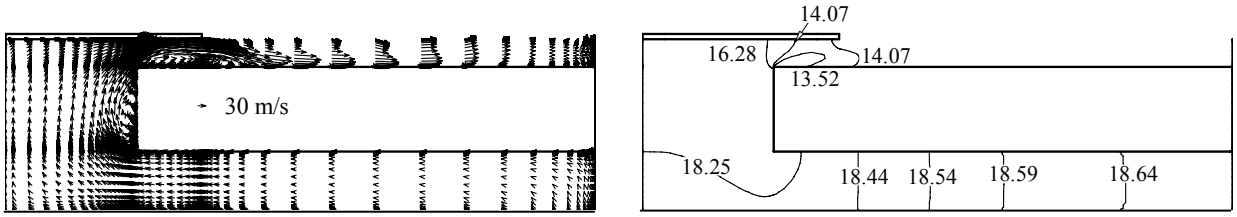

(b) ωt = 2.67

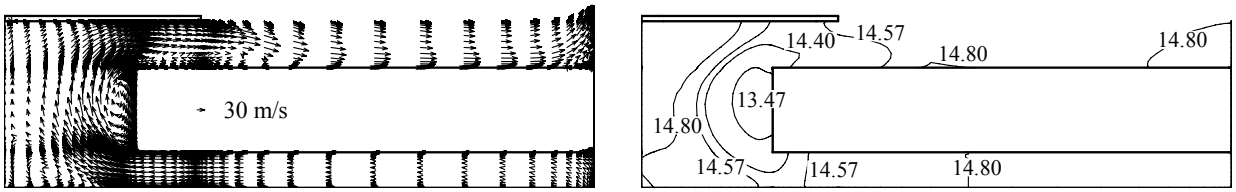

(c) ωt = 2.78

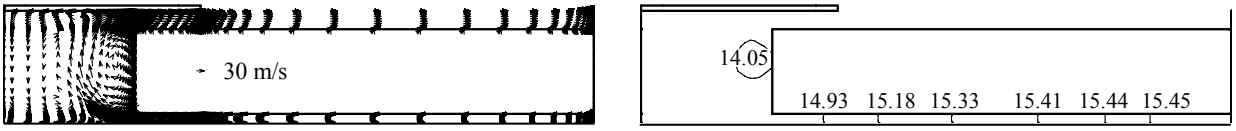

(d) ωt = 2.99.

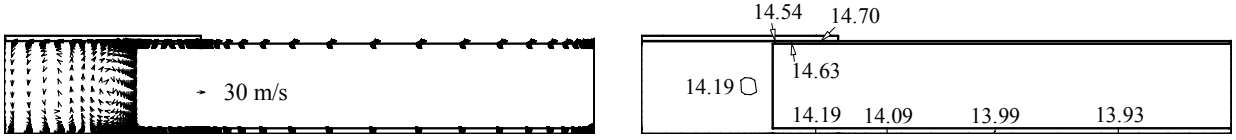

(e) ωt = 3.13.

Figure 4: Vector velocities and pressure contours during the discharge process.

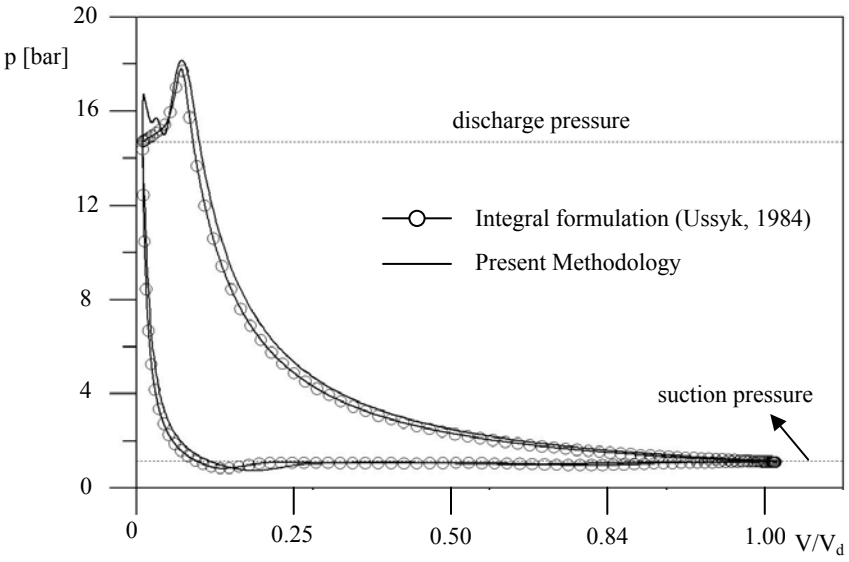

Figure 5: Comparison between integral and differential formulations.

5. CONCLUSIONS

A two-dimensional methodology has been proposed to simulate the complete compression cycle of reciprocating compressors, including the turbulent flow in the cylinder region and through the discharge valve. The contribution of turbulence to the flow transport was accounted for with the RNG k-ε model. The methodology was found to return a precise description of physical mechanisms that influence the compressor efficiency, such as pressure overshooting in the cylinder and backflow through the discharge valve. However, even for this two-dimensional model, the computational processing time is considered excessive for compressor design purposes.

REFERENCES

Deschamps, C.J., Prata, A.T. and Ferreira, R.T.S., 1996, Turbulent Flow through Reed Type Valves of Reciprocating Compressors, *Proc. ASME International Congress and Exposition - Symposium on the Analysis and Applications of Heat Pump & Refrigeration Systems*, Texas, USA: p. 151-161.

ElTahry, S.H., 1983, Kappa-Epsilon-Equation Model for Compressible Reciprocating-Engine Flows, *Journal of Energy* , v. 7, n. 4: p. 345-353.

Khalifa, E.H. and Liu, X., 1998, Analysis of Stiction Effect on the Dynamics of Compressor Suction Valve, *Proc. International Compressor Engineering Conference at Purdue*, USA, v. I: p. 87-92.

Matos, F.F.S., Prata, A.T., Deschamps, C.J., 2002, Numerical Simulation of the Dynamics of Reed Type Valves, *Proc. Compressor Engineering Conference at Purdue (CD-ROM)*, Indiana, USA, C15-2, 8 p.

Morel, T., Keribar, R., Comprehensive Model of a Reciprocating Compressor applicable to Component Design Issues, *Proc. International Compressor Engineering Conference*, West Lafayette, USA: p. 375-384.

Pérez-Segarra, C.D., Escanes, F., Oliva, 1994, Numerical Study of the Termal and Fluid Dynamic Behavior of Reciprocating Compressors, *Proc. Compressor Engineering Conference at Purdue*, Indiana, USA: p. 145-150.

Sarkar, S., Balakrishnan, L., 1990, Application of a Reynolds-Stress Turbulence Model to the Compressible Shear Layer, *ICASE Report 90-18*, NASA CR 182002.

Soedel, W., 1972, Introduction to Computer Simulation of Refrigerating Compressors, *Purdue University Short Courses*, West Lafayette, USA.

ACKNOWLEDGEMENT

This study forms part of a technical-scientific cooperation program between the Federal University of Santa Catarina and EMBRACO. Support from the Brazilian Research Council, CNPq, is also acknowledged.